ACS APPLIED MATERIALS & INTERFACES

Letter

www.acsami.org

N-Doped Crumpled Graphene Derived from Vapor Phase Deposition of PPy on Graphene Aerogel as an Efficient Oxygen Reduction Reaction Electrocatalyst

Meng Wang,[†] Jiazhao Wang,[‡] Yuyang Hou,[†] Dongqi Shi,[‡] David Wexler,[§] Simon D. Poynton,[∥] Robert C.T. Slade,[∥] Weimin Zhang,[⊥] Huakun Liu,[‡] and Jun Chen*,[†]

[†]ARC Centre of Excellence for Electromaterials Science, Intelligent Polymer Research Institute, Australian Institute of Innovative Materials, [‡]Institute for Superconducting and Electronic Materials, and [§]School of Mechanical, Materials and Mechatronic Engineering, University of Wollongong, Wollongong, NSW 2500, Australia

[∥]Department of Chemistry, University of Surrey, Guildford, Surrey GU2 7XH, United Kingdom

[⊥]Shanghai Sinopoly Batteries Research Institute, Shanghai, 200241, China

Supporting Information

ABSTRACT: Nitrogen-doped crumpled graphene (NCG) is successfully synthesized via vapor phase deposition of polypyrrole onto graphene aerogel followed by thermal treatment. The NCG was explored as an electrocatalyst for the oxygen reduction reaction, showing comparable electrocatalytic performance with the commercial Pt/C in alkaline membrane exchange fuel cells because of the well-regulated nitrogen doping and the robust micro-3D crumpled porous nanostructure.

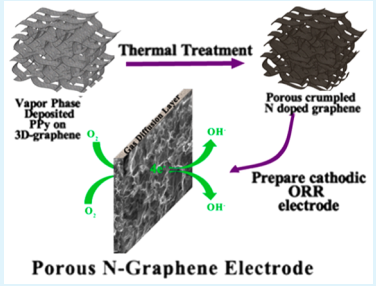

KEYWORDS: *nitrogen-doped graphene, vapor phase polymerization, oxygen reduction reaction, alkaline membrane fuel cell*

The oxygen reduction reaction (ORR) is recognized as a kinetically limited step in fuel cells and metal−air batteries because of its sluggish reaction mechanism.[1,2] Currently, platinum (Pt) is the commonly used electrocatalysts for the ORR; however, the high cost, susceptibility to fuel crossover, and poor stability have impeded its large-scale commercialization.[2,3] Recent studies in the heteroatom-doped (nitrogen,[1,4] boron,[5,6] sulfur,[1,4,7] phosphorus,[8] etc.) graphene suggest the doped graphene could potentially be used as metal-free, antipoison, and durable electrocatalysts to replace the high-cost Pt for the ORR. Chemically converted graphene,[9] owing to its ease of preparation and processing, has been extensively used for doping through various synthetic procedures, such as thermal annealing with nitrogen containing precursors,[1,4,6,10] hydrothermal reactions,[7,11,12] or nitrogen plasma treatment.[13] As a result of the doping, the spin density and charge distribution on carbon are altered, which could effectively improve the chemical and electronic properties over those of pristine graphene sheets thus enhancing the electrocatalytic performance for the ORR.[1,6,12,14] Chemically derived graphene sheets are vulnerable to stacking and aggregation, however, during reduction or drying processes because of the strong van der Waals and hydrogen bonding between water molecular and graphene sheets.[15] This irreversible stacking could decrease the specific surface area, cause the losses of active sites, and further hamper uniform doping, thereby compromising the overall properties of the electrocatalysts.[10,15]

In light of this, the design and preparation of three-dimensional (3D) porous doped graphene structures has become a key process in further widening the application of graphene for practical electrochemical devices. This is because the resultant 3D porous nanostructures could largely prevent the flat sheets from aggregating and restacking, giving them large surface areas and ample active sites for electrocatalytic reactions.[10,15,16] Despite many notable achievements in fabricating 3D porous doped graphene nanostructures,[1,7,11,16] there are still certain issues that need to be addressed, ranging from the complexity of the synthetic procedures to the post-treatment process. For example, structural template or interlayer spacer, such as silica nanoparticles, were usually employed to inhibit graphene sheets from stacking in preparing doped porous graphene structures; however, the additional cost and complexity of the template removal process has limited the feasibilities of these methods in practical production.[1,17] Recently, graphene hydrogel (GH) and graphene aerogel (GA, dehydrated GH), synthesized through a feasible self-assembly hydrothermal method, has been recognized a novel class of 3D macroporous graphene architectures,[15] and the hydrothermal doping during the formation of GH has been proposed as a feasible strategy for synthesis of 3D porous

Received: February 3, 2015
Accepted: March 24, 2015
Published: March 24, 2015

DOI: 10.1021/acsami.5b01025
ACS Appl. Mater. Interfaces 2015, 7, 7066−7072

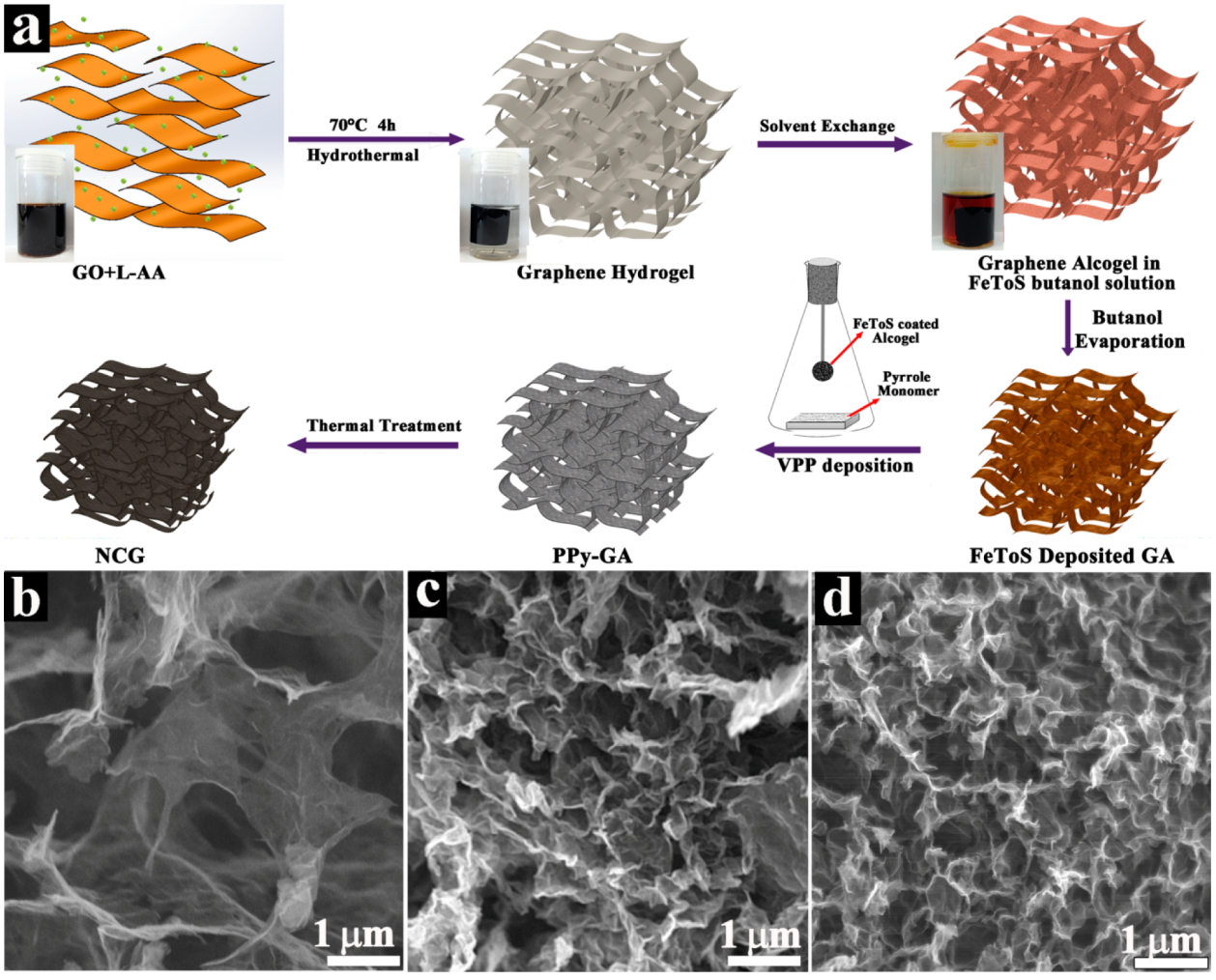

Figure 1. (a) Schematic preparation process of NCG based on a vapor phase polymerization method on graphene hydrogel. (b–d) SEM images collected during the preparation process to show a comparison between the (b) GA, (c) PPy-GA, and (d) NCG-1000.

doped graphene structures,[7] whereas the nitrogen configuration, which is crucial in determining catalyst performance, is beyond control.[7,12] Moreover, the resultant doped 3D monolithic graphene aerogels would be inevitably redispersed in post-treatment process for the preparation of oxygen reduction electrodes or membrane electrode assemblies (MEAs) of fuel cells or metal–air batteries, at which time the 3D monolithic porous structures would usually be demolished and the dispersed flat sheets would easily aggregate when they were dried, which would again minimize the specific surface areas and mass transfer channels of the electrocatalyst, thus decreasing the ORR performance.

In this report, we demonstrate the nitrogen-doped crumpled graphene (NCG) could be produced using GH as a starting material through the following steps: (i) vapor phase deposition of polypyrrole (PPy) film on the sheets of GA (PPy-GA), and (ii) introduction of the nitrogen species into graphene lattice via thermal annealing of the resultant PPy-GA to produce NCG. Vapor phase polymerization (VPP) is a well-established method in our group to produce inherently conducting polymer films with high conductivities and uniformity at the nanoscale on certain substrates.[18] The uniform PPy coating could work as interlayer spacer to effectively inhibit graphene sheets from stacking during the drying process and heat treatment, and could be simultaneously removed during doping process. In addition, uniform-doped crumpled graphene architecture could be produced in the preparation process and this porous structure could be well maintained during post-treatment process, which makes this NCG as promising electrocatalysts for ORR. The electrocatalytic performance toward ORR of the NCG was carefully examined in alkaline medium, where it showed comparable electrocatalytic activity with Pt/C (10 wt % Pt on Vulcan XC-72, E-Tek), but with better methanol tolerance and longer durability. Finally, we conduct anion exchange membrane fuel cell (AEMFC) tests to determine the real performance of our catalysts in a practical environment. To the best of our knowledge, this is the first AEMFC test using metal-free doped carbon materials as cathode catalysts. At the same loading level as the commercial Pt/C, our catalyst shows a maximum power output of 63 mW cm^{-2}, reaching 83% of the maximum power density of E-Tek Pt/C (76 mW cm^{-2}) suggesting its comparable performance with the Pt/C in practical environment These results would provide important information on the real performance of metal-free catalysts and therefore benefit research on metal-free electrocatalysts for the ORR.

The preparation process for NCG is illustrated in Figure 1a. The iron(III) p-toluenesulfonate (FeToS) was chosen as oxidizing agent for VPP growth of PPy owing to its unique advantage in producing uniform oxidant layer without

DOI: 10.1021/acsami.5b01025
ACS Appl. Mater. Interfaces 2015, 7, 7066–7072

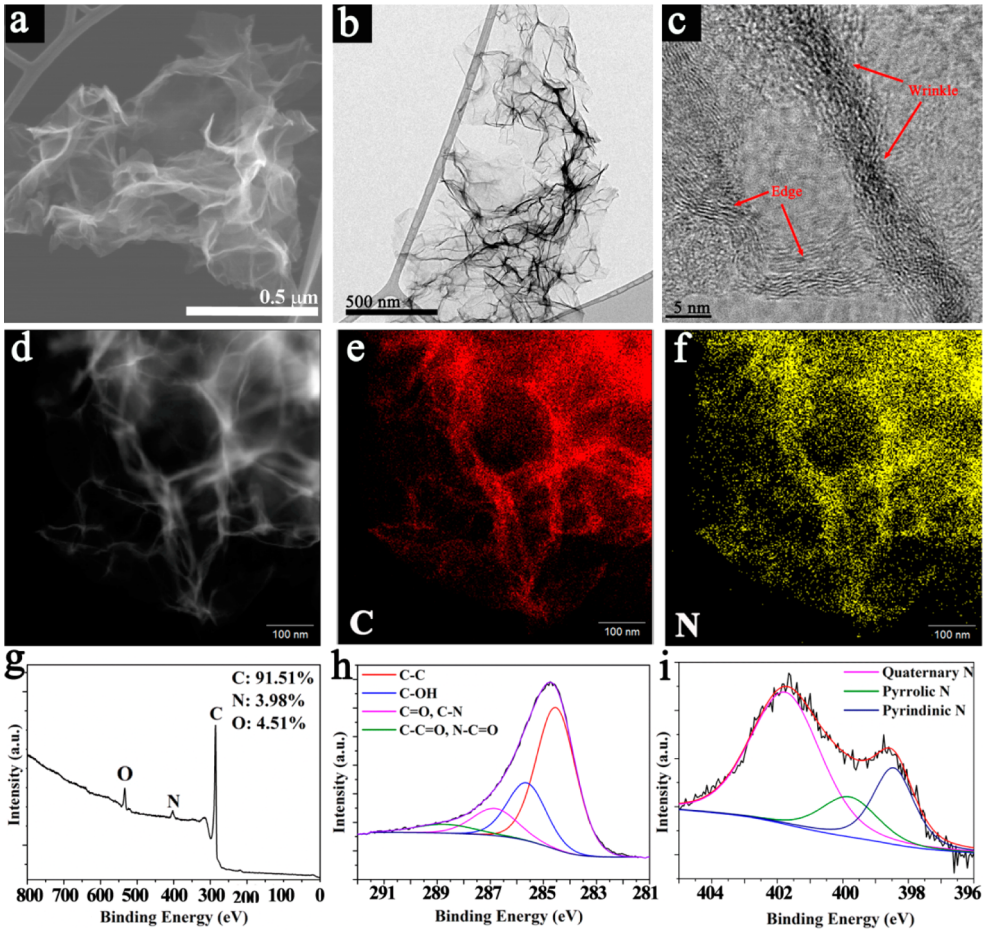

Figure 2. Characterization of NCG-1000: (a) SEM images, (b) TEM images, (c) HR-TEM images, (d) scanning transmission electron microscope (STEM). (e, f) EDS elemental mapping analysis of d: (e) carbon, (f) nitrogen. (g–i) XPS analysis: (g) survey spectrum. (h, i) corresponding high-resolution XPS spectra of (h) C 1s and (i) N 1s.

crystallization compared with other inorganic iron salts.[18,19] In a typical synthesis, GH was first produced and then submerged in ethanol (where the GH was converted into graphene alcogel) and FeToS butanol solution subsequently to allow exchange with the FeToS butanol solution into the resultant graphene alcogel. In the following step, the obtained FeToS butanol/graphene alcogel was directly annealed at 100 °C in order to quickly evaporate the butanol solvent without forming any crystallization and consequently a uniform FeToS oxidant layer would be generated onto the surface of graphene sheets. VPP was then carried out to grow PPy films on the aerogel (PPy-GA) by transferring the FeToS film-coated graphene alcogel into a VPP deposition chamber (Figure S1 in the Supporting Information) saturated with pyrrole monomer vapor and left for 1 h. After VPP, the PPy-coated graphene alcogel was washed with ethanol and water, and dried under ambient environment. During the drying process, the PPy-GA would be shrunk owing to the capillary force between the solvents and graphene sheets and as a result the crumpled sheets could be produced (Figure S2 insets in the Supporting Information). At last, the PPy-GA was annealed at a set of temperatures to convert into the NCG. At this step, the coated PPy would eventually decompose, providing a nitrogen source incorporating into the graphene lattice.

The morphology and structural transformation associated with the fabrication process between the pure GA, PPy-GA, and NCG were studied by scanning electron microscopy (SEM), as shown in Figure 1b–d. Compared with the GA (Figure 1b and Figure S2 in the Supporting Information), the pore sizes of the PPy-GA have become much smaller and the sheets are more wrinkled, which possibly arises from the shrinkage of the gel during solvent evaporation. More obviously, it can be seen that the graphene sheets become thicker and lose transparency indicating the successful deposition of PPy, which was very uniform across all the sheets (Figure S2 in the Supporting Information). Fourier transform infrared spectroscopy (FTIR, Figure S3a in the Supporting Information) and Raman spectroscopy, were first carried out showing the existence of PPy on GA with characteristic peaks of PPy clearly being identified in both spectra. The nitrogen content was about 5.9 at. % (atomic percentage, the same as below), as derived from X-ray photoelectron spectroscopy (XPS) (Figure S3c in the Supporting Information). The uniformity of the PPy coating was also investigated by transmission electron microscopy (TEM) (Figure S3d in the Supporting Information) and it can be seen that the PPy film is very uniform across all the graphene sheets, with no obvious PPy particles being observed, suggesting that the deposition was ultrathin and uniform.

After heat treatment, the 3D porous structure was well maintained, and the sheets of the NCG featured with abundant crumpled wrinkles (Figure 1d). It should be noted that the nitrogen doping level and the nitrogen configuration could be well-controlled by varying the annealing temperature. Generally, the nitrogen doping content is around 4 at %, decreasing

DOI: 10.1021/acsami.5b01025
ACS Appl. Mater. Interfaces 2015, 7, 7066–7072

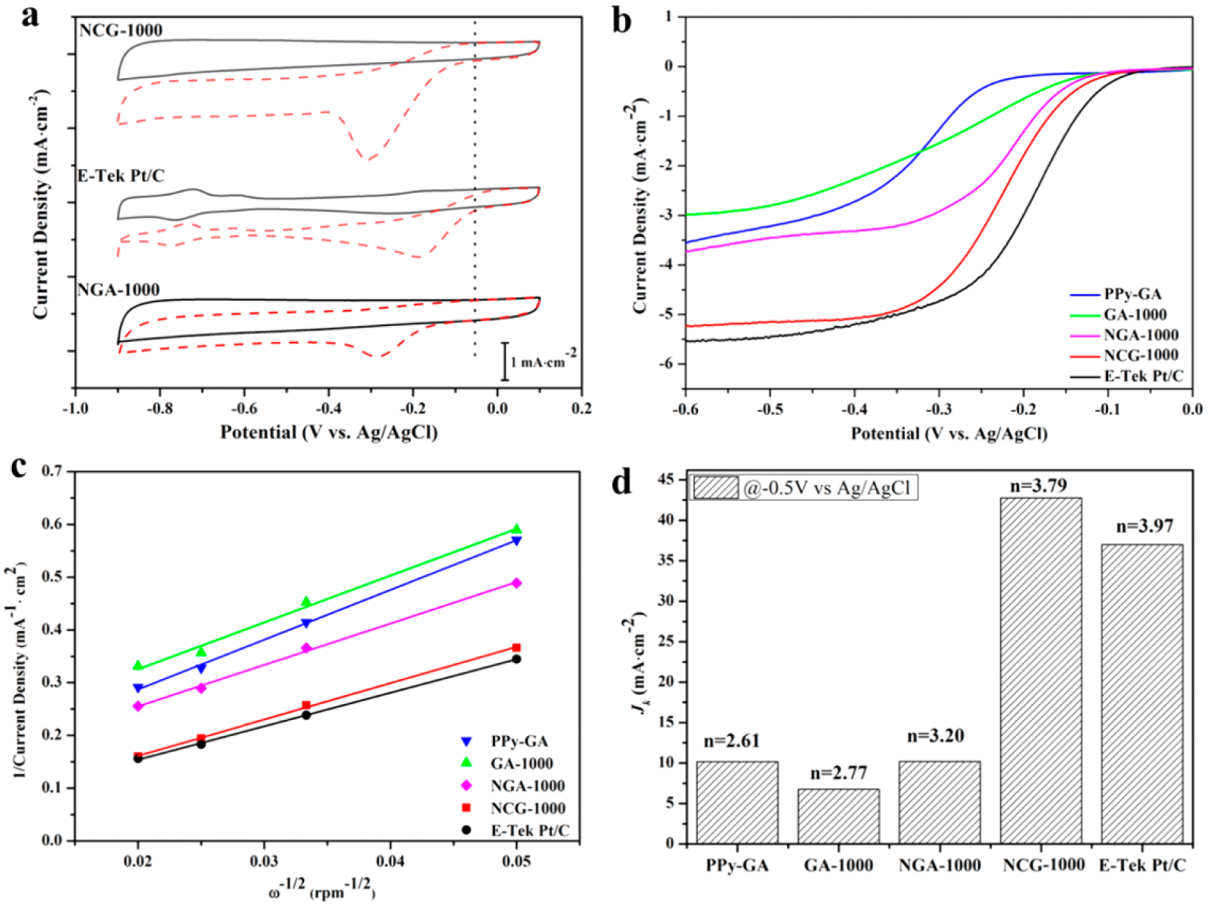

Figure 3. Comparison of the electrochemical catalytic performance of the synthesized NCG-1000, PPy-GA, GA-1000, NGA-1000, and the commercial available E-Tek Pt/C catalysts: (a) CV curves of the NCG-1000, NGA-1000 and E-Tek Pt/C electrocatalysts in N_2 (solid line) and O_2 (dashed lines) saturated electrolyte with a scan rate of 50 mV s^{-1}; the black dashed line indicates the onset potential of the NCG-1000. (b) Steady-state LSV curves at a rotating speed of 1600 rpm in O_2 saturated electrolyte. (c) Koutecky–Levich plots of the electrocatalysts at the potential of −0.5 V (vs Ag/AgCl). (d) Kinetic limiting current density (J_k) and the corresponding electron transfer number of the electrocatalysts.

with an increase in temperature, whereas with increasing temperature, the components of the quaternary N and pyridinic N could be largely increased (from initial 14% to 85% in the NCG-1000, Figures S4 and S5 and Table S1 in the Supporting Information). It shows that the content of pyrrolic form N of total N-doped in NCG-1000 has significantly decreased from initial 85% down to 15%. This indicates most N-doped has been doped into graphene lattice, not in the pyrrolic form. Combined with the results that the NCG annealed at 1000 °C, denoted as NCG-1000, showed the most positive onset potential and highest current density, which indicated the best electrocatalytic performance toward the ORR (Figure S6 in the Supporting Information), it is reasonable to believe that the quaternary N and pyridinic N, rather than the pyrrolic N, serve as catalytically active sites for the ORR, which is in good accordance with previous reports.[17] In this report, NCG-1000 was chosen for further characterization unless otherwise specified. Pure GA without the VPP process annealed at 1000 °C, denoted as GA-1000, and GA with a commonly used nitrogen source-urea annealed at 1000 °C, denoted as NGA-1000 (N content is 3.8%, Figure S7, see Supporting Information for detailed preparation process), were produced as control experiments to investigate the structural differences due to the VPP process and to study the impacts on electrochemical properties due to different nitrogen doping methods.

It is worthwhile to note that all of the three carbon electrocatalysts (GA-1000, NGA-1000, and NCG-1000) maintained with porous 3D structure after heat treatment (Figure S8a–c in the Supporting Information); however, for practicable applications, electrocatalysts need to be dispersed via sonication in order to apply these electrocatalysts on membrane electrodes or other electrodes. After sonication and deposition, the NCG-1000, with most of the sheets crumpled, still exhibits a highly porous structure (Figure S8d in the Supporting Information). In contrast, the 3D and porous macrostructure of the GA-1000 and NGA-1000 were mostly demolished, and the majority of the sheets were flat and stacked on the membrane electrode during the electrode preparation process (Figure S8e, f in the Supporting Information). These observations clearly suggest that the synthesized NCG-1000, manifest unique robust crumpled micro-3D nanostructure and this robust porous feature could be well-maintained during postprocessing. Therefore, it is expected that the NCG-1000 would be an ideal candidate for the ORR because of the ample O_2 and ion transfer channels, as well as the greater number of active sites on the ORR electrodes. This was later proven by the following electrochemical tests.

The detailed morphologies of the NCG-1000 was initially studied via SEM, confirming a micro-3D structure composed with crumpled folded graphene sheets was produced in the NCG-1000 (Figure 2a). TEM further displays that the porous

DOI: 10.1021/acsami.5b01025
ACS Appl. Mater. Interfaces 2015, 7, 7066–7072

structure of NCG-1000 is constructed with numerous curves and wrinkles (Figure 2b) and these wrinkled features were also investigated by high resolution TEM (HRTEM) as shown in Figure 2c. Typical graphite crystalline structure could be seen on the sheets edges, indicating that the sheets in the NCG-1000 were somewhat stacked during the formation of GA and the heat treatments, while on the wrinkles, no visible graphite crystalline structures could be detected, implying these wrinkles were caused by crumpling of graphene sheets rather than stacking of graphene.[11,18] Figure 2d shows a scanning transmission electron microscope (STEM) image of NCG-1000, which again confirms the presence of porous 3D crumpled sheets, as discussed above. The uniformity of nitrogen doping was evidenced by energy-dispersive X-ray spectroscopy (EDS) mapping analysis, as is shown in Figure 2e, f. Homogenous nitrogen doping was realized, as is clear from the element mapping, suggesting the effectiveness of this method in producing uniform doping. The nature of the doping was further studied by XPS, showing that about 4 at. % nitrogen is incorporated into the graphene lattice (Figure 2g). The high-resolution C 1s peak could be fitted into several spectral peaks: C−C at 284.8 eV, C−O at 285.9 eV, C═O or C−N at 287.1 eV, and C−C═O at 289.0 eV (Figure 2h). Compared with the GA-1000, the peak area at 287.1 eV of NCG-1000 was increased, indicating that the nitrogen was doped into the graphene lattice (Figure S9 in the Supporting Information).[15] The nitrogen configuration was investigated from the high-resolution N 1s spectrum (Figure 2i), which could be fitted to three peaks of pyridinic N (398.5 eV), pyrrolic N (399.8 eV), and quaternary N (401.5 eV).[3,11] Compared with the nitrogen configurations in PPy-GA, nitrogen atoms were rearranged through heat treatment from pyrrolic N to quaternary N and pyridinic N, possibly because the pyrrolic N was not stable at high temperature.[17] Such a rearrangement is beneficial for the electrocatalysts as the quaternary and pyridinic N are more active in catalyzing the ORR than the pyrrolic N, as aforementioned. Raman spectroscopy further confirmed the incorporation of nitrogen into the graphene lattice (Figure S10 in the Supporting Information). For instance the up-shifted D band as well as the increase in the intensity ratio of the D to the G peak (I_D/I_G) of NCG-1000, compared with the GA and GA-1000, suggest that the structural disorder was increased, which was ascribed to the doping of nitrogen into the graphene sheets.[6,11]

Cyclic voltammetry (CV) curves were obtained and used for a preliminary study of the electrocatalytic oxygen reduction properties of the synthesized electrocatalysts (Figure 3a). As shown in Figure 3a, a quasi-rectangular featureless voltammetric current within the potential range between −0.9 and 0.1 V was observed for NCG-1000 in N_2-saturated solution, which corresponds to a result of the typical supercapacitance effect on porous carbon materials.[6,16] In contrast, when O_2 saturated electrolyte was used, a well-defined ORR peak centered at −0.31 V with a current density of −2.9 mA cm^{-2}, was detected, and the onset potential (the potential at which oxygen reduction commences) was at about −0.05 V, which was comparable with that of the Pt/C (−0.01 V) and significantly higher than those of the GA-1000 (−0.13 V) and the PPy-GA (−0.21 V), indicating that the nitrogen doping could effectively enhance the ORR performance (Figure S11 in the Supporting Information). In comparison with the NGA-1000 electrode which showed an onset potential of −0.12 V, the higher onset potential of the NCG-1000 suggested the dominant role of the nitrogen configuration, as well as the porous structures on the electrocatalytic performance of the electrocatalysts, which also indicated the advantages of this method in producing well-controlled nitrogen-doped crumpled graphene over the conventional protocols.

To gain insight into the ORR activities and kinetics of the electrocatalysts, steady state ORR polarization curves of the E-Tek Pt/C, PPy-GA, GA-1000, NGA-1000, and NCG-1000 electrocatalysts were recorded respectively (Figure 3b). The curves on GA-1000 and PPy-GA showed a slow current increase and no current plateau, revealing their poor performance toward the ORR.[6,20] In contrast, a well-defined diffusion-limiting current region from −0.6 to −0.35 V and a mixed kinetic-diffusion control region from −0.08 to −0.35 V were observed on the NCG-1000, which is very similar to the behavior of the Pt/C, indicating its comparable activity toward the ORR compared with the commercial Pt/C. As a comparison, the NGA-1000 displayed a similar plateau but with a much lower diffusion limiting current density, owing to limited active sites exposing at the reaction zone between the bulk electrode and electrolyte and the lack of sufficient ion and mass transfer channels on the electrodes. To identify the ORR activity of the electrocatalysts, the half-wave potential ($E_{1/2}$), at which the current is a half of the limiting current, was calculated. For the NCG-1000, the $E_{1/2}$ is −0.223 V, which is about 30 mV lower than that of Pt/C (−0.193 V) and much more positive than those of GA-1000 (−0.295 V) and PPy-GA (−0.351 V). The above comparisons clearly indicate that the crumpled porous NCG-1000 manifested significant improvement in electro-catalyzing O_2 in an alkaline medium compared with NGA-1000, suggesting that this doping method could effectively increase the electrocatalytic performance of the catalysts, which may be ascribed to the well maintained porous structure during the post treatment process.

To obtain the kinetics of the ORR, we also collected steady-state ORR polarization curves at various rotation speeds, and corresponding Koutecky−Levich (K-L) plots were drafted from the ORR polarization curves. Figure 3c shows the K-L plots of various samples at −0.5 V (vs Ag/AgCl) and the plots of all the samples show good linearity. Noticeably, the NCG-1000 showed a much higher ORR current, which is close to that of the commercial Pt/C and significantly higher than those of GA-1000, PPy-GA, and NGA-1000 at all rotation speeds, which is a further indication of the outstanding ORR catalytic performance on the crumpled doped graphene electrodes as compared with other three carbon materials. The electron-transfer numbers (n) and the kinetic limiting current (J_k) of all the samples at −0.5 V (vs Ag/AgCl) were calculated according to the slopes of the linear fitted K-L plots on the basis of the K-L equation (Figure 3c, d). The NCG-1000 exhibited much higher electron transfer efficiency as well as the kinetic limiting current over the GA-1000, PPy-GA, and NGA-1000. In comparison with the E-Tek Pt/C, the J_k for the NCG-1000 was even much higher than that of the Pt/C and was comparable to or even higher than most of recently reported doped graphene electrodes (Table S2 in the Supporting Information), suggesting the unique superiority of this method for producing highly efficient metal-free electrocatalyst for the ORR by controllably varying the nitrogen configuration and the generation of enduring porous structure.

The fuel tolerance of the cathode catalysts is critical in the real application for fuel cells, because the relatively small methanol or other fuel molecules such as methanol would cross

DOI: 10.1021/acsami.5b01025
ACS Appl. Mater. Interfaces 2015, 7, 7066−7072

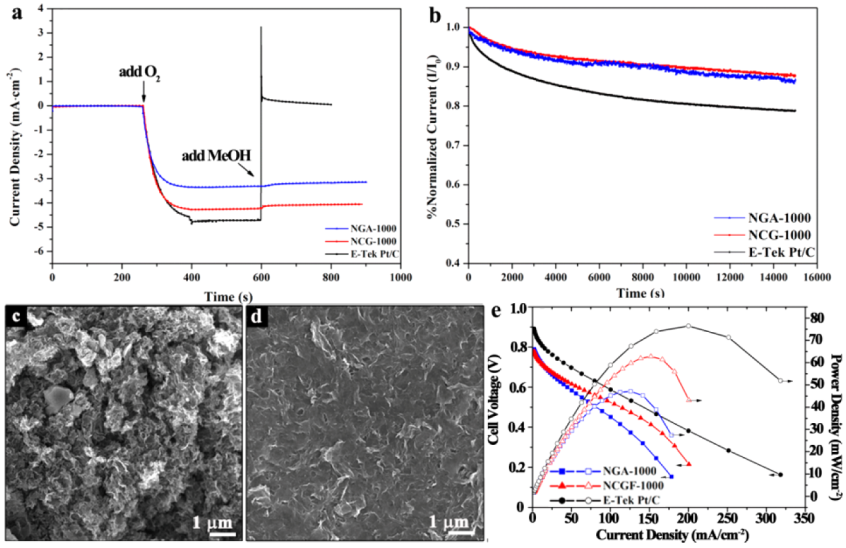

Figure 4. Chronoamperometric responses at −0.3 V (vs Ag/AgCl) of the NGA-1000, NCG-1000, and E-Tek Pt/C at the rotation speed of 1600 rpm (a) with oxygen and methanol (1 M) added at about 250 and 600 s respectively, (b) in O2 saturated electrolyte up to 15000 s at −0.3 V (vs Ag/AgCl). (c, d) SEM image of the catalysts layers on gas diffusion layer (GDL) with (c) NCG-1000 and (d) NGA-1000 as electrocatalysts. (e) Current density curves and power density curves of a single AEMFC test using E-Tek Pt/C, NGA-1000, and NCG-1000 as cathode catalysts.

through the membrane and react with the catalysts in the cathodes, which will cause mixed potentials and thus reducing the cell efficiency.[1,6,21] To this end, the selectivity of NCG-1000, NGA-1000, and commercial Pt/C were compared through chronoamperometric measurements at the rotation speed of 1600 rpm at −0.3 V (vs Ag/AgCl) with the subsequent introduction of oxygen and methanol, as displayed in Figure 4a. The introduction of oxygen led to a significant increase in the current density, and a stable current was attained for the three catalysts, revealing that their ORR performance were comparative. After the addition of methanol, however, a distinct change on current was observed for the Pt/C catalyst, indicating that methanol oxidation had occurred, i.e., the selectivity of the Pt/C was poor. In contrast, for the NGA-1000 and NCG-1000, the current remained nearly unchanged after the addition of methanol, reflecting their superior selectivity and better methanol tolerance due to the nature of nitrogen-doped carbon materials. The durability of these catalysts was also assessed by the chronoamperometric technique at −0.3 V (vs Ag/AgCl) (Figure 4b).[1,6] During the long-term testing (up to 15 000 s), a similar current loss was observed for the NCG-1000 and NGA-1000 suggesting their durability were almost the same, whereas for the commercial Pt/C, a dramatic current loss was observed, indicating that the NCG-1000 had superior advantages over the commercial Pt/C when used as long-term running electrocatalysts.

The AEMFC tests were finally conducted in order to obtain the real performance of the catalysts in a practical environment. To the best of our knowledge, the testing of metal-free nitrogen doped materials in a real anion membrane single cell has rarely been reported, possibly because of the lack of an anion exchange membrane and anion exchange ionomer and the relatively poor ORR activities of the nonmetal carbon electrocatalysts compared with the metal−nitrogen-carbon electrocatalysts[22,23] or noble metal catalysts.[24] The morphologies of the NCG-1000 catalyst layers on GDL are shown in Figure 4c, displaying that the microporous structure of NCG-1000 is well kept on the GDL. However, in contrast, the porous structure of NGA-1000 was mostly demolished and most sheets were relatively flat with some area stacking together on the GDL (Figure 4d). The merit of the porous structure of NCG-1000 electrode is expected to increase the capacitance and the electroactive surface area (ESA) of the electrode, which was also confirmed through the in situ CV measurement of the two electrodes under identical conditions (Figure S12 in the Supporting Information). The higher ESA and porous structure would accelerate the reaction between electroactive materials and electrocatalysts and the mass transport rate in a real AEMFC and these were further evidenced by the polarization curves of the single cell on these two catalysts, as shown in Figure 4e. It can be seen at low current density area (<50 mA cm^{-2}), the polarization curves for the NCG-1000 and NGA-1000 are almost the same. However, at the higher polarization potential, the NCG-1000 delivers a much higher current than the NGA-1000. The reason may be ascribed to the open and porous structure on the electrode, which could facilitate oxygen and ion transport, thereby enhancing the performance of the electrode. This comparison illustrated the significance of the porous structure in producing high-performance ORR catalysts for real fuel cell. Further comparisons were made against the commercial E-Tek Pt/C at the same mass loading level (2 mg cm^{-2}) under identical testing conditions. At the practicable operating potential (~0.6 V), the current density for the NCG-1000 was about 60 mA cm^{-2}, which is about 63% of the E-Tek Pt/C (95 mA cm^{-2}) and the maximum power density for the NCG-1000 was about 63 mW cm^{-2}, reaching 83% of the maximum power density of E-Tek Pt/C (76 mW cm^{-2}). These comparisons clearly indicate that the power output of the NCG-1000 is comparable with that of the Pt/C, revealing that it could work as an efficient metal-free electrocatalyst under practicable working conditions. Moreover, no virtual changes on the microstructures of the NCG-1000 catalyst layer were observed after single-cell performance test, suggesting significant robust porous structure of the NCG-1000 (Figure S13 in the Supporting Information).

In summary, we have demonstrated that the uniform nitrogen-doped crumpled graphene could be produced through vapor phase deposition of PPy on GA (PPy-GA) following by

DOI: 10.1021/acsami.5b01025
ACS Appl. Mater. Interfaces 2015, 7, 7066−7072

thermal treatment in this report. The uniform doping nature, well-regulated nitrogen configuration, and the robust micro-3D crumpled porous nanostructure, which could be well-maintained after the post processing in preparing ORR electrodes or membrane electrodes, endow the catalyst with excellent catalytic performance toward the ORR. The AEMFC tests also provide convincing evidence that these metal-free nitrogen doped carbon materials could work as comparable efficient catalysts, comparable to the Pt/C, under real operation condition thus providing further confidence for developing metal-free catalysts for the next-generation fuel cells. This work will help further understand the mechanism of nitrogen doping in ORR electrocatalytic performance and would benefit the development of conducting polymer-graphene composites and metal-free doped graphene catalysts for the applications in the electrocatalysis, energy storage devices, and energy conversion systems.

■ ASSOCIATED CONTENT

Ⓢ Supporting Information

Supplimentary materials include: (i) Experimental Section with detail information on materials preparation, characterization, and device assembly and investigation; (ii) supplementary Figures and Tables with quality discussion that is not mentioned in main text; and (iii) references that are cited in the Supporting Information. This material is available free of charge via the Internet at http://pubs.acs.org/.

■ AUTHOR INFORMATION

Corresponding Author

* E-mail: junc@uow.edu.au.

Notes

The authors declare no competing financial interest.

■ ACKNOWLEDGMENTS

The authors thank Dr. Tania Silver for critical proof reading and acknowledge financial support from the Australian Research Council (DP140100401) and the use of the facilities within the UOW Electron Microscopy Centre. Work at the University of Surrey was funded under EPSRC contract EP/H025340/1

■ REFERENCES

(1) Liang, J.; Jiao, Y.; Jaroniec, M.; Qiao, S. Z. Sulfur and Nitrogen Dual-doped Mesoporous Graphene Electrocatalyst for Oxygen Reduction with Synergistically Enhanced Performance. *Angew. Chem., Int. Ed.* **2012**, *51*, 11496−11500.

(2) Gong, K.; Du, F.; Xia, Z.; Durstock, M.; Dai, L. Nitrogen-Doped Carbon Nanotube Arrays with High Electrocatalytic Activity for Oxygen Reduction. *Science* **2009**, *323*, 760−764.

(3) Lai, L.; Potts, J. R.; Zhan, D.; Wang, L.; Poh, C. K.; Tang, C.; Gong, H.; Shen, Z.; Lin, J.; Ruoff, R. S. Exploration of The Active Center Structure of Nitrogen-Doped Graphene-Based Catalysts For Oxygen Reduction Reaction. *Energy Environ. Sci.* **2012**, *5*, 7936−7942.

(4) Wang, X.; Wang, J.; Wang, D.; Dou, S.; Ma, Z.; Wu, J.; Tao, L.; Shen, A.; Ouyang, C.; Liu, Q.; Wang, S. One-pot Synthesis of Nitrogen and Sulfur Co-doped Graphene as Efficient Metal-free Electrocatalysts for the Oxygen Reduction Reaction. *Chem. Commun.* **2014**, *50*, 4839−4842.

(5) Zheng, Y.; Jiao, Y.; Ge, L.; Jaroniec, M.; Qiao, S. Z. Two-step Boron and Nitrogen Doping in Graphene for Enhanced Synergistic Catalysis. *Angew. Chem., Int. Ed.* **2013**, *52*, 3110−3116.

(6) Wang, S.; Zhang, L.; Xia, Z.; Roy, A.; Chang, D. W.; Baek, J. B.; Dai, L. BCN Graphene as Efficient Metal-free Electrocatalyst for the Oxygen Reduction Reaction. *Angew. Chem., Int. Ed.* **2012**, *51*, 4209−4212.

(7) Su, Y.; Zhang, Y.; Zhuang, X.; Li, S.; Wu, D.; Zhang, F.; Feng, X. Low-temperature Synthesis of Nitrogen/Sulfur Co-doped Three-Dimensional Graphene Frameworks as Efficient Metal-free Electrocatalyst for Oxygen Reduction Reaction. *Carbon* **2013**, *62*, 296−301.

(8) Zhang, C.; Mahmood, N.; Yin, H.; Liu, F.; Hou, Y. Synthesis of Phosphorus-doped Graphene and Its Multifunctional Applications for Oxygen Reduction Reaction and Lithium Ion Batteries. *Adv. Mater.* **2013**, *25*, 4932−4937.

(9) Hummers, W. S.; Offeman, R. E. Preparation of Graphitic Oxide. *J. Am. Chem. Soc.* **1958**, *80*, 1339−1339.

(10) Wen, Z.; Wang, X.; Mao, S.; Bo, Z.; Kim, H.; Cui, S.; Lu, G.; Feng, X.; Chen, J. Crumpled Nitrogen-Doped Graphene Nanosheets with Ultrahigh Pore Volume for High-Performance Supercapacitor. *Adv. Mater.* **2012**, *24*, 5610−5616.

(11) Wu, Z. S.; Winter, A.; Chen, L.; Sun, Y.; Turchanin, A.; Feng, X.; Müllen, K. Three-Dimensional Nitrogen and Boron Co-doped Graphene for High-performance All-solid-state Supercapacitors. *Adv. Mater.* **2012**, *24*, 5130−5135.

(12) Wang, H.; Xie, M.; Thia, L.; Fisher, A.; Wang, X. Strategies on the Design of Nitrogen-Doped Graphene. *J. Phys. Chem. Lett.* **2013**, *5*, 119−125.

(13) Wang, Y.; Shao, Y.; Matson, D. W.; Li, J.; Lin, Y. Nitrogen-Doped Graphene and Its Application in Electrochemical Biosensing. *ACS Nano* **2010**, *4*, 1790−1798.

(14) Zhang, L.; Xia, Z. Mechanisms of Oxygen Reduction Reaction on Nitrogen-doped Graphene for Fuel Cells. *J. Phys. Chem. C* **2011**, *115*, 11170−11176.

(15) Xu, Y.; Sheng, K.; Li, C.; Shi, G. Self-assembled Graphene Hydrogel via a One-step Hydrothermal Process. *ACS Nano* **2010**, *4*, 4324−4330.

(16) Mao, S.; Wen, Z.; Huang, T.; Hou, Y.; Chen, J. High-performance Bi-functional Electrocatalysts of 3D Crumpled Graphene-Cobalt Oxide Nanohybrids for Oxygen Reduction and Evolution Reactions. *Energy Environ. Sci.* **2014**, *7*, 609−616.

(17) Yang, S.; Zhi, L.; Tang, K.; Feng, X.; Maier, J.; Muellen, K. Efficient Synthesis of Heteroatom (N or S)-Doped Graphene Based on Ultrathin Graphene Oxide-Porous Silica Sheets for Oxygen Reduction Reactions. *Adv. Funct. Mater.* **2012**, *22*, 3634−3640.

(18) Winther-Jensen, B.; Chen, J.; West, K.; Wallace, G. Vapor Phase Polymerization of Pyrrole and Thiophene Using Iron(III) Sulfonates as Oxidizing Agents. *Macromolecules* **2004**, *37*, 5930−5935.

(19) Chen, J.; Wang, J. Z.; Minett, A. I.; Liu, Y.; Lynam, C.; Liu, H.; Wallace, G. G. Carbon Nanotube Network Modified Carbon Fibre Paper for Li-ion Batteries. *Energy Environ. Sci.* **2009**, *2*, 393−396.

(20) Zheng, Y.; Jiao, Y.; Chen, J.; Liu, J.; Liang, J.; Du, A.; Zhang, W.; Zhu, Z.; Smith, S. C.; Jaroniec, M.; Lu, G. Q.; Qiao, S. Z. Nanoporous Graphitic-C3N4@Carbon Metal-Free Electrocatalysts for Highly Efficient Oxygen Reduction. *J. Am. Chem. Soc.* **2011**, *133*, 20116−20119.

(21) Liu, M.; Lu, Y.; Chen, W. PdAg Nanorings Supported on Graphene Nanosheets: Highly Methanol-Tolerant Cathode Electrocatalyst for Alkaline Fuel Cells. *Adv. Funct. Mater.* **2013**, *23*, 1289−1296.

(22) Li, Q.; Cao, R.; Cho, J.; Wu, G., Nanocarbon Electrocatalysts for Oxygen Reduction in Alkaline Media for Advanced Energy Conversion and Storage. *Adv. Energy Mater.* **2014**, *4*, DOI:10.1002/aenm.201301415.

(23) He, Q.; Li, Q.; Khene, S.; Ren, X.; López-Suárez, F. E.; Lozano-Castelló, D.; Bueno-López, A.; Wu, G. High-Loading Cobalt Oxide Coupled with Nitrogen-Doped Graphene for Oxygen Reduction in Anion-Exchange-Membrane Alkaline Fuel Cells. *J. Phys. Chem. C* **2013**, *117*, 8697−8707.

(24) Wang, M.; Zhang, W.; Wang, J.-Z.; Wexler, D.; Poynton, S. D.; Slade, R. C. T.; Kun-Liu, H.; Winther-Jenson, B.; Kerr, R.; Shi, D.; Chen, J. PdNi Hollow Nanoparticles for Improved Electrocatalytic Oxygen Reduction in Alkaline Environments. *ACS Appl. Mater. Interfaces* **2013**, *5*, 12708−12715.

DOI: 10.1021/acsami.5b01025
ACS Appl. Mater. Interfaces 2015, 7, 7066−7072